

Iterative Solutions for Electromagnetic Fields at Perfectly Reflective and Transmissive Interfaces Using Clifford Algebra and the Multidimensional Cauchy Integral

Ajalawit Chantaveerod and Andrew D. Seagar, *Member, IEEE*

Abstract—A technique is presented for calculating the solution of Maxwell’s equations using a CFIE based on the Cauchy integral and formulated in the guise of Clifford algebra. This formulation has a geometric interpretation leading to an iterative method of solution which is easily proven as convergent and correct for both perfectly reflective and perfectly transmissive interfaces. Simple test cases involving a cubic boundary and plane wave and dipole sources are used to investigate the numerical performance of the method.

Index Terms—Boundary integral, Cauchy integral, Clifford algebra, Maxwell’s equations.

I. INTRODUCTION

CAST INTO integral form Maxwell’s differential equations yield integral equations both throughout three-dimensional regions and over two-dimensional surfaces. The surface integrals lead to a variety of boundary integral equations [1]–[3] relating potentials, fields and/or sources. Formulation of the boundary integral equations typically employs a scalar Green’s function to invert differential equations involving one or more potentials. If equations involving fields rather than potentials are required the integral equations involving potentials can be differentiated, converting potentials into the corresponding fields. Within this general approach specific choices of method lead to different formulations such as the EFIE (electric field integral equation [4]–[6]) and the MFIE (magnetic field integral equation [4], [6]–[8]). Using the EFIE or the MFIE it is possible to solve for the scattered fields from conducting bodies. It is also possible to combine these two approaches into a single CFIE (combined field integral equation [4], [9]–[12]) and solve simultaneously for both electric and magnetic field.

Numerical solutions of electric, magnetic and combined field equations are typically based on the method of moments [13]–[15], with which a system matrix can be constructed

for a field (solution) vector. Inversion of the system is often carried iteratively [14]–[16] by whatever technique seems to suit any given problem. Iterative techniques which guarantee convergence to the correct solution are clearly preferable to those that do not.

A great deal of freedom exists in exactly how to formulate integral equation techniques firstly at the level of the equations themselves and secondly at the level of the numerical solution. Formulation of integral equations can be carried either by using potentials and differentiations or by avoiding them altogether. One approach of the latter kind uses a multidimensional version of the Cauchy integral [17] to invert differential equations in the form of fields directly into the corresponding boundary integral equations [18]. This multidimensional Cauchy integral was not used when the approaches based on Green’s functions were first developed for the simple reason that, at that time (cf. [19]), it had yet to be discovered. Only recently [17] has this alternative approach appeared in the mathematical literature.

From a mathematical viewpoint, the method is based on extending the properties of analytic functions of complex variables in the plane, to multiple dimensions [20] as what are called *monogenic* functions of Clifford variables in N -dimensional space, where $N \geq 2$. (Of course, in electromagnetism only $N = 4$ dimensions are required, three for space and one for time or frequency). Such a generalization of complex variables into multiple dimensions has long been sought, engineers well recognizing their invaluable properties for solving field problems which conform to a two-dimensional planar geometry. That the generalization has proved somewhat elusive is in part because it is not to be found amongst the familiar mathematical tools of real or complex variables, algebra and arithmetic. Rather, the generalization is to be found amongst the (less familiar) tools of *Clifford* variables, algebra and arithmetic. These tools were actually developed for the specific purpose of making Maxwell’s equations easier to solve a long time ago by Clifford [21], a student of Maxwell’s [22], but were for some reason or the other, overlooked. However, a growing interest in applying Clifford’s algebra to problems in mathematical physics including electromagnetism, gravitation and multiparticle quantum mechanics [23] has appeared within the last few years.

Regardless of origin, the key point now for the engineer is that this particular approach leads to an alternative method for solving Maxwell’s equations as a CFIE (where ‘C’ could stand equally well for “combined” or “Clifford”). The Clifford algebra itself presents few problems. Apart from being non-com-

Manuscript received July 24, 2008; revised January 29, 2009. First published September 11, 2009; current version published November 04, 2009. The work of A. Chantaveerod was supported by a scholarship from the Faculty of Engineering at Walailak University which funded his work within the Department of Electrical Engineering, Chulalongkorn University.

A. Chantaveerod is with the Department of Electrical Engineering, Chulalongkorn University, Bangkok 10330, Thailand (e-mail: cyodchai@gmail.com).

A. D. Seagar is with the Department of Telecommunication, Rajamangala University of Technology Srivijaya, Songkhla 90000, Thailand (e-mail: dr_andrew_seagar@ieee.org).

Digital Object Identifier 10.1109/TAP.2009.2032099

mutative, it is only marginally more complicated than complex algebra.

The approach involving the Cauchy integral and Clifford algebra bears a formal similarity to integral methods involving Green's functions. However, they are by no means directly equivalent. The kernel for the Cauchy integral solves a first order differential equation whereas the Green's functions solve a second order differential equation. The singularities that appear in each differ, for example $(-1)e^{-ikr}/4\pi r$ for the Green's function in the frequency domain and $\{-(\vec{r}/r^2) + ik(i\epsilon_0 - \vec{r}/r)\}e^{-ikr}/4\pi r$ for the Cauchy kernel (see [24]).

The Cauchy integral is known to apply to Lipschitz surfaces [18], [25], i.e. those with sharp corners and edges, such as cubes and wedges. It correctly accommodates fields which approach infinity at such points (cf. [26], [27]) provided that the basis functions for the fields on the boundary are chosen correctly. The functional analysis has been carried in two cases: one for fields on the boundary in the L^2 (square integrable) functional space [18], [25], and one for functions in a more complicated functional space denoted in [28] as \mathcal{X}^2 . The second choice ensures that the field *off* the boundary is locally square integrable (i.e. finite energy, L^2).

Although mathematicians have proved to their satisfaction that solutions to Maxwell's equations exist within the framework of Clifford algebra and the multidimensional Cauchy integral, the task of demonstrating any such solutions has been left to others. The aim of this paper is to undertake that task, to report a viable algorithm which in theory converges to the correct solution, and to demonstrate its numerical performance.

Section II makes a few preliminary remarks about the use of Clifford algebra from the viewpoint of application to electromagnetism. Sections III and IV introduce the key elements developed by the mathematicians. Of particular importance are the Cauchy extension, the Cauchy integral and the Hardy projections in Section IV. These tools provide a method writing and manipulating what are otherwise integral equations as simple algebraic ones. Sections V and VI show first how Maxwell's equations are written in terms of these tools, and then how the solution can be obtained by geometrical construction. The geometry here is in an affine functional space (i.e., in a Banach space) rather than a space of ordinary points, but for the most part the same rules apply (cf. [29]). The main theoretical contribution of this paper is the iterative solution presented in Section VI-B. Section VII describes numerical tests designed to investigate the performance of the iterative solution in terms of convergence and accuracy. The main experimental contribution of this paper are the results in Section VIII given by applying the tests to two particular cases: a cube illuminated from the outside by a plane wave, and from the inside by a Hertzian dipole. Section IX shows results when the technique is applied to one simple application, and Section X concludes with a discussion.

II. PRELIMINARIES

In using the multidimensional Cauchy integral to solve problems involving Maxwell's equations it is expeditious (although not strictly essential) to cast Maxwell's equations, the magnetic and electric field vectors and the divergence and curl differential operators into the framework of Clifford algebra rather than using them in the framework of vector calculus. The frequency

domain form of Maxwell's equations becomes what is known as the Maxwell-Dirac equation. The two fields and the two differential operators manifest themselves as bivector and vector parts respectively of two four dimensional Clifford numbers (or variables): the single electromagnetic field u and the single k -Dirac operator D_k . For a detailed introduction to Clifford algebras see (for example) the book [30].

Four dimensional Clifford numbers take the general form

$$\begin{aligned} a = & a_0 + a_1 e_0 + a_2 e_1 + a_3 e_2 + a_4 e_3 + a_5 e_0 e_1 + a_6 e_0 e_2 \\ & + a_7 e_1 e_2 + a_8 e_0 e_3 + a_9 e_1 e_3 + a_{10} e_2 e_3 + a_{11} e_0 e_1 e_2 \\ & + a_{12} e_0 e_1 e_3 + a_{13} e_0 e_2 e_3 + a_{14} e_1 e_2 e_3 + a_{15} e_0 e_1 e_2 e_3. \end{aligned} \quad (1)$$

The a_i are complex-valued numeric coefficients. The e_i are symbolic entities known as Clifford units. For the purposes of electromagnetism the Clifford units e_i play the role of four Cartesian basis vectors, the (compound) units $e_i e_j$ play the role of bivectors (oriented areas), the $e_i e_j e_k$ play the role of trivectors (oriented volumes), and $e_0 e_1 e_2 e_3$ plays the role of the four dimensional pseudo-scalar.

The arithmetic operations required are those of addition and multiplication. Addition $a+b$ is simply a matter of adding all the corresponding complex coefficients $a_i + b_i$. Multiplication ab entails use of the distributive law of multiplication over addition. The 256 terms produced are then further reduced by applying the two rules for multiplication of Clifford units

$$e_i e_j = \begin{cases} -1 & \text{if } i = j \\ -e_j e_i & \text{if } i \neq j. \end{cases} \quad (2)$$

The first rule has the same characteristics as the rule $i^2 = -1$ for squaring the unit imaginary number i . The second rule has the same anticommutative property as the rule for the vector cross product, $x \times y = -y \times x$.

The electromagnetic field is written in Cartesian form as a four-dimensional Clifford bivector (cf. [30]–[32])

$$u = \sqrt{\mu} H \sigma + i \sqrt{\epsilon} E e_0 \quad (3)$$

where $H = H_x e_1 + H_y e_2 + H_z e_3$ and $E = E_x e_1 + E_y e_2 + E_z e_3$, the constant $\sigma = -e_1 e_2 e_3$, and i is the unit imaginary number. The four Clifford units e_0, e_1, e_2, e_3 play the role of temporal (e_0) and spatial (e_1, e_2, e_3) dimensions (cf. [24]). The vector differential operators *div* and *curl* are written as a three dimensional Clifford vector

$$D = e_1 \frac{\partial}{\partial x} + e_2 \frac{\partial}{\partial y} + e_3 \frac{\partial}{\partial z} \quad (4)$$

called the Dirac derivative or the Clifford gradient. In the frequency domain an additional dimension is used to accommodate the wavenumber $k = \omega/\sqrt{\mu\epsilon}$, giving the four dimensional k -Dirac operator $D_k = D - k e_0$. For a point source δ_0 at the origin the fundamental solution F_k of the k -Dirac operator (i.e. solution to the equation $D_k F_k = \delta_0$) at a point p is

$$F_k(p) = \left\{ -\frac{1}{r^2} p + ik \left(i e_0 - \frac{1}{r} p \right) \right\} \frac{e^{-ikr}}{4\pi r} \quad (5)$$

where $r = |p|$. The frequency domain version of the homogeneous form of Maxwell's equations (which are the ones used

in the boundary formulation here) are written as the Maxwell-Dirac or k -Dirac equation [18], [24]

$$D_k u = 0. \tag{6}$$

Here the electromagnetic field u of (3) is a monogenic function since the source term on the right is zero. Such a field could represent the total field in a region without sources, or some aspect of a field in a region containing sources (such as the field reflected from or transmitted through a boundary). If the inhomogeneous equation is required (i.e. with sources) there is a non-zero term on the right hand side. In that case the field u is no longer a monogenic function.

III. FIELDS ON BOUNDARY

When using vector calculus the electromagnetic field is described as separate electric and magnetic field vectors

$$\begin{cases} \vec{E} = E_x \vec{a}_x + E_y \vec{a}_y + E_z \vec{a}_z \\ \vec{H} = H_x \vec{a}_x + H_y \vec{a}_y + H_z \vec{a}_z \end{cases} \tag{7}$$

On the boundary at the interface between two homogeneous regions with different electrical properties, the field vectors exhibit certain discontinuities. These discontinuities are described by relationships (cf. [33]) between the fields on the two sides of the interface

$$\begin{cases} \vec{n} \cdot (\epsilon_2 \vec{E}_2 - \epsilon_1 \vec{E}_1) = \rho_s \\ \vec{n} \times (\vec{H}_2 - \vec{H}_1) = \vec{J}_s \\ \vec{n} \times (\vec{E}_2 - \vec{E}_1) = 0 \\ \vec{n} \cdot (\mu_2 \vec{H}_2 - \mu_1 \vec{H}_1) = 0 \end{cases} \tag{8}$$

where \vec{J}_s and ρ_s are the electric surface current density and surface charge density respectively, where \vec{n} is a unit vector normal to the interface, and where ϵ_1, μ_1 and ϵ_2, μ_2 are the electric permittivity and permeability in the two regions. The material properties μ and ϵ take complex scalar values. This accommodates lossy material in the frequency domain as a non-zero imaginary part of ϵ , but excludes anisotropic media.

Here, Maxwell's equations are solved using the multidimensional Cauchy integral, which can be expressed mathematically most directly when set in a framework of Clifford algebra (see [17]), not vector calculus. For the boundary conditions, the normal and the tangential components of the field are written not in terms of the scalar (dot) and vector (cross) products in (8), but instead in terms of two projection operators

$$\begin{cases} Q^+ v = \frac{1}{2}(I + Q)v \\ Q^- v = \frac{1}{2}(I - Q)v \end{cases} \tag{9}$$

derived both from the same reflection operator Q , where $Qv = nvn$. The reflection operator Q produces an image of a vector $v = v_x e_1 + v_y e_2 + v_z e_3$ reflected in the tangent plane to a boundary with a unit normal vector $n = n_x e_1 + n_y e_2 + n_z e_3$. Combining the vector with its mirror image as in (9) cancels either the normal part of the vector v_n leaving only the tangential part v_t , or *vice versa*.

When applied to the bivector electromagnetic field u in (3), the result is a mixture of normal (E_n, H_n) and tangential (E_t, H_t) components of both electric and magnetic fields

$$w = \begin{cases} Q^+ u = \sqrt{\mu} H_t \sigma + i\sqrt{\epsilon} E_n e_0 \\ Q^- u = \sqrt{\mu} H_n \sigma + i\sqrt{\epsilon} E_t e_0 \end{cases} \tag{10}$$

A second level of projection operators

$$\begin{cases} Sw = \frac{1}{2}(I + T)w \\ Tw = \frac{1}{2}(I - T)w \end{cases} \tag{11}$$

derived both from the same reflection operator T , where $Tw = \sigma w \sigma$, separates the mixture of normal and tangential components into all four parts by cancelling either the space-like (σ) part of the bivector w leaving only the time-like (e_0) part, or *vice versa*. The four boundary conditions in (8) can then be written in Clifford algebra using combinations of the T, S, Q^+, Q^- operators. For example

$$\begin{cases} TQ^+(\sqrt{\epsilon_2}u_2 - \sqrt{\epsilon_1}u_1) = 0 \\ SQ^+\left(\frac{u_2}{\sqrt{\mu_2}} - \frac{u_1}{\sqrt{\mu_1}}\right) = 0 \\ TQ^-\left(\frac{u_2}{\sqrt{\epsilon_2}} - \frac{u_1}{\sqrt{\epsilon_1}}\right) = 0 \\ SQ^-(\sqrt{\mu_2}u_2 - \sqrt{\mu_1}u_1) = 0 \end{cases} \tag{12}$$

if there are no sources on the boundary and the conductivity is everywhere finite.

IV. HARDY PROJECTIONS

The boundary value theorem [18] relates integrals of functions a, b over a closed boundary Σ to integrals of derivatives of those functions throughout the interior region Ω^+ . Stokes' theorem and the divergence theorem are special cases of the boundary theorem. When the Dirac operator D (4) is used instead of curl and divergence operators the boundary value theorem takes the form

$$\int_{\Sigma} b(q)n(q)a(q)d\sigma(q) = \int_{\Omega^+} \{(bD)(q)a(q) + b(q)(Da)(q)\} dx \tag{13}$$

where q is a Clifford number representing a point on the boundary Σ or within its interior Ω^+ , $n(q)$ is a Clifford number representing the outward unit normal, and $d\sigma(q)$ and dx are the differential measures of area on the boundary and volume in the interior respectively.

In the special case when $a(q)$ is replaced by a monogenic function $u(q)$ and $b(q)$ is replaced by the fundamental solution of the k -Dirac operator: $b(q) = E_k(q - p) = -F_k(p - q)$, then the boundary value theorem reduces to the integral equation formulation [24]

$$u(p) = \int_{\Sigma} E_k(q - p)n(q)u(q)d\sigma(q). \tag{14}$$

This formula is known as the reproducing formula because the value $u(p)$ of a monogenic (source free) electromagnetic field

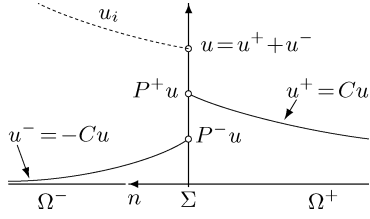


Fig. 1. Cauchy extensions u^\pm and Hardy projections $P^\pm u$ for function u on boundary Σ with unit normal n .

at a point inside a closed boundary can be reconstructed from its value $u(q)$ on the boundary.

The reproducing formula is a single-sided formula, producing only the value inside the boundary. Patching together two copies of the reproducing formula, one for the outside and one for the inside regions, gives the Cauchy extension operator [18], [24]

$$\begin{aligned} Cu(p) &= \int_{\Sigma} E_k(q-p)n(q)u(q)d\sigma(q) \\ &= \begin{cases} u^+(p \in \Omega^+) \\ -u^-(p \in \Omega^-) \end{cases} \end{aligned} \quad (15)$$

where p represents a point placed inside either Ω^+ or Ω^- and the function $u(q)$ on the boundary Σ can take any value; it need no longer be the trace of a monogenic function. Given $u(q)$ the Cauchy extension produces two monogenic fields propagating away from the boundary: u^+ into Ω^+ and u^- into Ω^- as shown in Fig. 1.

In electromagnetic problems the monogenic fields u^+ and u^- play the role of fields transmitted through and reflected from the boundary. The source of the incident field, from which u^+ and u^- are generated, could be somewhere in either Ω^+ or Ω^- . Supposing that the source is in Ω^- , the broken curve u_i in Fig. 1 now represents the incident field. The incident field is related to the function u on the boundary through the boundary conditions (8) or (12) as extracted by the Q^\pm projection operators in (9) and (10). The total field in Ω^- is the sum of incident and reflected fields $u_2 = u_i + u^-$, whereas the total field in Ω^+ is the transmitted field by itself, $u_1 = u^+$.

The difference of the two extensions for two points, p_- in Ω^- and p_+ in Ω^+ , in the limit as they approach the same point p on the boundary from opposite sides retrieves the boundary function u as a sum of two parts

$$\begin{aligned} u(p) &= \lim_{p_+ \rightarrow p} Cu(p_+) - \lim_{p_- \rightarrow p} Cu(p_-) \\ &= u^+(p) + u^-(p) = P^+u(p) + P^-u(p) \end{aligned} \quad (16)$$

with the two Hardy projection operators P^+ and P^- introduced to represent the two limits (see [18], [34]). Applying the Hardy projection operator P^+ to the function u on the boundary extracts the trace on the boundary of the transmitted field u^+ , and applying the Hardy projection operator P^- extracts the trace on the boundary of the reflected field u^- . The whole of the reflected field u^- and the transmitted field u^+ can be recovered using the Cauchy extension operator (15).

Note that it is the sense of the normal that determines which is the inside and which is the outside, rather than the converse. The sense of the normal can be chosen without regard to the particular geometry of any given application. Here the source

TABLE I
HARDY AND CAUCHY INTEGRAL OPERATORS

| field u | Hardy projection P^+u | P^-u | Cauchy integral $C_\Sigma u$ |
|--------------|----------------------------|--------|---------------------------------|
| u^+ | u | 0 | u |
| u^- | 0 | u | $-u$ |
| $u^+ + u^-$ | u^+ | u^- | $u^+ - u^-$ |

has been chosen in Ω^- , the region into which the normal points. To put the source and the incident field on the other side of the boundary without changing any equations is simply a matter of reflecting Fig. 1 about the vertical axis, effectively reversing the normal, all three fields, and all labels.

With point p on the boundary Σ itself, the Cauchy integral operator (see again [18])

$$\begin{aligned} C_\Sigma u(p) &= 2 \text{ p.v. } \int_{\Sigma} E_k(q-p)n(q)u(q)d\sigma(q) \\ &= u^+(p) - u^-(p) \end{aligned} \quad (17)$$

gives the difference of the two fields. With the sum (as in (16)) and difference of the two fields known, each part can be separated

$$\begin{cases} u^+ = \frac{1}{2}(I + C_\Sigma)u = P^+u \\ u^- = \frac{1}{2}(I - C_\Sigma)u = P^-u \end{cases} \quad (18)$$

Table I summarizes the effects of the Cauchy integral and Hardy operators on three particular fields. The first is the case where there is no reflection, i.e. a perfectly transparent object. In this case there is no reflected field, so that on the boundary $u \equiv u^+$. The second case is for a perfectly reflecting object (conductor). Now there is no transmitted field, so that $u \equiv u^-$. The third case is for an object which is partially transmissive and partially reflective. In this case both transmitted and reflected fields are non-zero, and the function u on the boundary is the value of their sum. Note that the Hardy projections play the role of decomposing the function on the boundary into its transmitted and reflected components, which may according to circumstance amount to the whole field, part of the field, or zero.

V. INTEGRAL EQUATIONS FOR FIELDS ON BOUNDARY

Fig. 2 shows an electromagnetic field travelling from Ω^- into Ω^+ , where the material properties are ϵ_-, μ_- and ϵ_+, μ_+ respectively. The field is shown split into three components

$$\begin{cases} u_i = \sqrt{\mu_-}H_i\sigma + i\sqrt{\epsilon_-}E_i e_0 \\ u^- = \sqrt{\mu_-}H^- \sigma + i\sqrt{\epsilon_-}E^- e_0 \\ u^+ = \sqrt{\mu_+}H^+ \sigma + i\sqrt{\epsilon_+}E^+ e_0 \end{cases} \quad (19)$$

where u_i , u^- and u^+ are four-dimensional Clifford bivectors representing incident, reflected and transmitted fields respectively. The total fields as in (8) or (12) are $u_2 = u_i + u^-$ in Ω^- and $u_1 = u^+$ in Ω^+ .

The cases where one of the fields is zero are the most simple. For perfectly reflecting objects there is no transmitted field u^+ , so that $u_2 = u_i + u^-$ and $u_1 = 0$. Applying the Hardy projections (18) as in Table I gives

$$\begin{cases} P^+u = 0 \\ P^-u = u = u^- \end{cases} \quad (20)$$

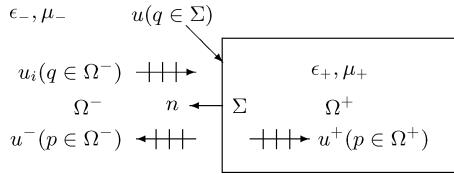


Fig. 2. Components of field transmitted (u^+) and reflected (u^-) at interface between two different materials. Incident field u_i originates from a source in Ω^- .

For perfectly transparent objects there is no reflected field u^- , so that $u_2 = u_i$ and $u_1 = u^+$. Applying the Hardy projections to this case gives

$$\begin{cases} P^+u = u = u^+ \\ P^-u = 0. \end{cases} \quad (21)$$

Cases where there is partial transmission and reflection are more involved. See [25] for details.

Equations (20) and (21) are integral equations which relate the various components of the field on the boundary Σ . Their nature as integral equations is seen by examining the Hardy projections as written in (18) in terms of the Cauchy integral, and then by referring to the nature of the Cauchy integral in (17). Equations (20) and (21) play the same role as integral equations for fields that integral equations involving Green's functions play for potentials.

In electromagnetism, (20) applies to scattering problems, which are of practical importance in the design of antennas and waveguides. Equation (21) is also of importance. Its role lies in extending radiation patterns (as, for example, measured in an anechoic chamber) from the near field into the far field.

VI. GEOMETRIC SOLUTION

For cases of perfect transmission or reflection, solution of Maxwell's equations uses the integral equations in (20) or (21), along with boundary conditions from (8) or (12). For perfect transmission any of the boundary conditions can be used, because there are no sources induced on the boundary. For perfect reflection only the bottom two equations can be used because charge and current sources of unknown value are induced. Adopting here the bottom two equations gives

$$\begin{cases} P^-u = u \\ Q^-u = g \end{cases} \quad (22)$$

for perfect reflection, and adopting the top two equations gives

$$\begin{cases} P^+u = u \\ Q^+u = f \end{cases} \quad (23)$$

for perfect transmission. The boundary conditions $f = Q^+u_i$ and $g = -Q^-u_i$ are, as in (10), whatever mixture of normal and tangential components of the incident electric and magnetic fields is appropriate to the given problem.

Surface currents play no role in (22) and (23), and appear nowhere in the solution. It is for that reason it is possible to use the technique for objects which are not perfect electrical conductors just as easily as for objects which are perfect electrical conductors.

In order to visualise the solutions to (22) and (23) it is useful to represent them in a geometric form. Since P^\pm and Q^\pm are

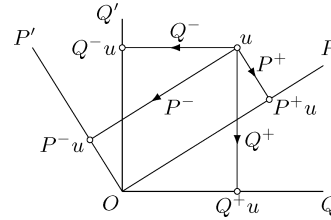


Fig. 3. Function u represented as point in Banach space with two coordinate systems OP, OP' and OQ, OQ' .

operators which take the projections of functions rather than points, the appropriate geometrical space to use is one of functions u , as shown in Fig. 3, rather than points.

Any function u in this space can be represented in terms of two components Q^+u and Q^-u lying on coordinate axes OQ and OQ' respectively, or equally well in terms of two components P^+u and P^-u lying on axes OP and OP' . The two Q^\pm or P^\pm components behave like vectors and add directly to reconstruct the function u . The space behaves as if two-dimensional because the function can be fully reconstructed from only two components.

Although the figure as drawn appears to be either Euclidean for points or Hilbert for functions, this is not the case. The space lacks an inner product, so that angles (including right angles) have no meaning. Any figure which can be derived from Fig. 3 by a non-singular shearing operation is completely equivalent. Such spaces for points are called affine and for functions, as here, are called Banach spaces.

In Banach space the simultaneous equations in (22) and (23) can be drawn as in Fig. 4(a) and 4(b) respectively. Translating (22) into the language of geometry reads on the first line "the solution u lies on the OP' axis" and on the second line "the solution u lies on a line through the function g on the OQ' axis parallel to the OQ axis." Translating (23) reads on the first line "the solution u lies on the OP axis" and on the second line "the solution u lies on a line through the function f on the OQ axis parallel to the OQ' axis."

It is one of the strengths of the approach adopted here, using Clifford algebra and the multidimensional Cauchy integral, that the solution of Maxwell's equations for a perfectly reflective or transmissive objects of any shape is reduced to finding the intersection of two straight lines.

Testing any method of finding the intersection can in principle be carried on either the problem of Fig. 4(a) or Fig. 4(b). However, in practice Fig. 4(b) offers two advantages. The advantages come from reasons which are not geometric, since the two geometric problems are equivalent (rotating Fig. 4(b) by ninety degrees maps it onto Fig. 4(a)). The reasons are in the numerical representation of the field u , and in the independent knowledge of the actual solution.

For Lipschitz surfaces it is normally necessary to choose a basis which accommodates singularities at edges and corners, since the field can take infinite value at those places. However, for Fig. 4(b) the object is completely transparent so the field is everywhere (except at the source) regular and finite. That means a simpler basis can be chosen, one which cannot support singular field behaviour, without sacrificing accuracy. For perfectly reflecting objects of arbitrary shape, it is normally necessary to

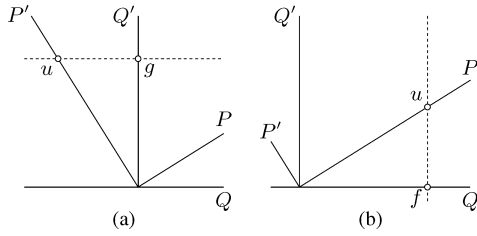


Fig. 4. Solution of Maxwell's equations as intersection in Banach space of dotted line through boundary conditions f, g and coordinate axis OP, OP' for cases of (a) perfect reflection and (b) perfect transmission.

calculate the reflected field $u = u^-$ numerically. Indeed, that is the very aim of this work. However, testing any new numerical method is only as good as the accuracy to which the true solution is known. For Fig. 4(b), the solution $u = u^+$ is known with zero error in advance, being simply the same as the incident field. That makes it possible to establish the accuracy of the numerical method with a higher degree of precision.

The approach here is therefore to test the method of finding the solution to Maxwell's equations by intersection of two straight lines in Banach space, on Fig. 4(b). Note in advance (see Section VI-B) that any implementation for a solution to (23) can be altered to produce a corresponding implementation for a solution to (22) by changing only two signs in the original. However maintaining the accuracy of that derived solution also depends on upgrading the basis functions from the ones chosen here to ones which accommodate singularities.

A. Formal Solution

Consider now in detail the solution to the perfect transmission problem (23) and Fig. 4(b).

Adding two components of a vector reconstructs the vector, so that $Q^+ + Q^- = I$, where I is the identity. Substituting into (23) gives

$$\begin{cases} P^+(Q^+ + Q^-)u = u \\ Q^+u = f \end{cases} \quad (24)$$

But now from the boundary condition $Q^+u = f$

$$P^+f + P^+Q^-u = u \quad (25)$$

Reference to Fig. 5 shows the geometric meaning of (25) as adding (as vectors along the OP axis) the two functions P^+f and P^+Q^-u to reconstruct the function u (also as a vector along the OP axis). All trilaterals in Fig. 5 which appear by casual inspection to be similar are indeed similar. This holds even after any non-singular shearing operation. It therefore also follows geometrically, immediately by inspection, that the sum of these two functions does indeed reconstruct the solution u .

Rearranging (25)

$$P^+f = (I - P^+Q^-)u \quad (26)$$

$$u = (I - P^+Q^-)^{-1}P^+f \quad (27)$$

now gives a formal solution in terms of the inverse of a compound operator $I - P^+Q^-$.

Note that (26) is *not* in the form of a Fredholm integral equation. Writing (26) in full integral form shows that the operator $(I - P^+Q^-)$ embeds u with non-commutative multiplication

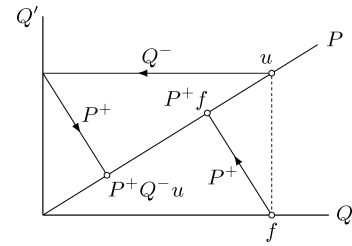


Fig. 5. Solution u in Banach space as vectorial sum of projections P^+f, P^+Q^-u along axis OP .

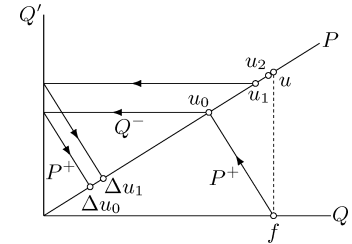


Fig. 6. Iterative solution. Adding correction Δu_0 to initial estimate u_0 gives improved estimate u_1 , and adding Δu_1 to u_0 gives u_2 .

from both sides. For a Fredholm integral equation the multiplication is from one side only. Whereas a direct matrix inverse style of solution for a discrete approximation to a Fredholm integral equation is possible, the same cannot be said for (26). The formal solution as written in (27) is symbolic only, and should not be mistaken for some kind of matrix inverse.

B. Iterative Solution

The solution for u in (27) need not involve a direct inversion of the compound operator $I - P^+Q^-$. An iterative procedure can be used, as shown in Fig. 6.

An initial estimate

$$u_0 = P^+f \quad (28)$$

is obtained by projecting the boundary conditions f onto the OP axis. A correction $\Delta u_0 = P^+Q^-u_0$ is calculated by projecting u_0 first onto the OQ' axis and then back onto the OP axis. A new estimate $u_1 = u_0 + \Delta u_0$ is obtained by adding the correction to initial estimate. As a second iteration, an improved correction $\Delta u_1 = P^+Q^-u_1$ is used to give a better estimate $u_2 = u_0 + \Delta u_1$. Note that the correction is always added to the initial estimate u_0 , not to the most recent estimate. The general form of the k^{th} estimate u_k is

$$u_k = u_0 + P^+Q^-u_{k-1} = \sum_{m=0}^k (P^+Q^-)^m u_0 \quad (29)$$

The solution takes the form of a Neumann iteration, with initial guess u_0 calculated directly from the boundary conditions f . A different field $u'_0 = P^+v$ could also be chosen for an initial guess. This would make sense if it is known that u'_0 is closer to the solution than u_0 .

The difference between consecutive estimates is

$$u_k - u_{k-1} = (P^+Q^-)^k u_0 \quad (30)$$

which, as shown in Fig. 7, approaches zero as k approaches infinity at a rate proportional to the size of the difference.

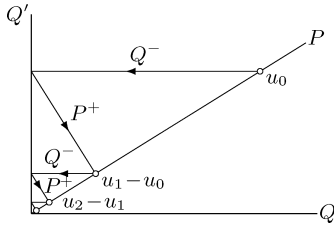


Fig. 7. The difference $u_k - u_{k-1}$ between consecutive estimates of solution u approaching zero as the iteration proceeds.

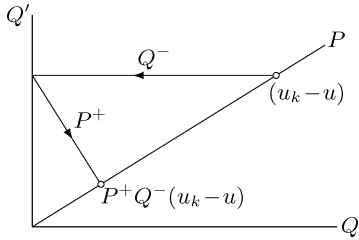


Fig. 8. The difference between estimate u_k and solution u is the same after projections P^+Q^- only if $u_k - u = 0$, showing convergence to the correct solution $u_k = u$.

In principle, the difference reduces to zero after an infinite number of iterations. At that stage $u_k = u_{k-1}$, so that

$$u_k = u_0 + P^+Q^-u_{k-1} = u_0 + P^+Q^-u_k \quad (31)$$

The difference from the correct solution u can be found by subtracting (25)

$$(u_k - u) = P^+Q^-(u_k - u) \quad (32)$$

which by inspection of Fig. 8 can only be true if $u_k - u$ is sitting at the origin, so that $u_k = u$. It therefore follows that the iterative method in (28) and (29) converges and, furthermore, converges to the correct solution.

A solution for the case of perfect reflection can be developed in exactly the same way. For perfect reflection, the solution is given formally by

$$u = (I - P^-Q^+)^{-1}P^-g \quad (33)$$

and the iterative solution is

$$\begin{cases} u_0 = P^-g \\ u_k = \sum_{m=0}^k (P^-Q^+)^m u_0 \end{cases} \quad (34)$$

Convergence to the correct solution is assured for perfect reflection in the same way as for perfect transmission.

In both cases the iterative solution can be obtained by expanding the inverse of the compound operator $I - X$ in the formal solution as a binomial series $(I - X)^{-1} = \sum_{m=0}^{\infty} X^m$. Convergence of the binomial series follows from the properties of the operator X . Note in the case of Fig. 7 that $X = P^+Q^-$ and for any function $x \neq 0$ on the OP axis that $|P^+Q^-x| < |Ix| = |x|$ since P^+Q^-x is closer to the origin. That is always true as long as P^\pm and Q^\pm (as here) are some kind of projection operators.

Note that any *implementation* of the transmissive solution can be altered to produce an implementation of the reflective solu-

TABLE II
ANGULAR RATIOS ON CUBE

| position | ratio τ^\pm | |
|----------|------------------|----------------|
| | interior field | exterior field |
| corner | 1/4 | 7/4 |
| edge | 1/2 | 3/2 |
| smooth | 1 | 1 |

tion by changing only two signs in the whole procedure: the plus sign inside $P^+ = (1/2)(I + C_\Sigma)$ to minus, giving P^- , and the minus sign inside $Q^- = (1/2)(I - Q)$ to plus, giving Q^+ . Doing so converts the equations for the transmissive solution (28) and (29) directly into the equations for the reflective solution (34), as long as the appropriate boundary conditions are used.

VII. METHODOLOGY

A cubic boundary Σ is used to test the iterative solution of Fig. 6, and (28) and (29). For this boundary minor modifications in the Cauchy integral and Hardy projections are required at the corners and edges. Equations (17) and (18) strictly apply only to points on smooth surfaces. In the case of points on edges and corners for the problem of perfect transmission, the equations should be written more generally as

$$\begin{aligned} C_\Sigma u(p) &= 2 \text{p.v.} \int_{\Sigma} E_k(q-p)n(q)u(q)d\sigma(q) \\ &= \tau^+ u^+(p) - \tau^- u^-(p) \end{aligned} \quad (35)$$

and

$$\begin{cases} u^+ = \frac{1}{2}(\tau^- I + C_\Sigma)u = P^+u \\ u^- = \frac{1}{2}(\tau^+ I - C_\Sigma)u = P^-u \end{cases} \quad (36)$$

Here, the parameter $\tau^\pm = \theta_i/\theta_{ii}$ is the ratio of two angles: (i) the angle on the side of the boundary indicated by the superscript $x \in \{+, -\}$ subtended to a point on the boundary, and (ii) the angle on either side of the tangent plane at the same point. The ratios at edges and corners, when calculating the Hardy projections for the interior and exterior fields, are as listed in Table II.

The surface of the cube is divided into $N = 6M^2$ square elements of equal size. The Cauchy integral is calculated as a sum of smaller integrals $F_j(p)$ over each element Σ_j

$$\begin{cases} C_\Sigma u(p) = \sum_{j=1}^N F_j(p) \\ F_j(p) = 2\text{p.v.} \int_{\Sigma_j} E_k(q-p)n(q)u(q)d\sigma(q) \end{cases} \quad (37)$$

The field u on each element is approximated by a bilinear function

$$u(q) = u(q(x, y)) = \sum_{i=1}^4 A_{ij} f_i(x, y) \quad (38)$$

in a local coordinate system x, y . The coefficients A_{ij} are Clifford bivectors which represent the values of the field at the four corners. Multiplying by the scalar functions f_i

$$f_i(x, y) = \left[\frac{1}{2} \pm \left(\frac{x}{\ell} - \frac{1}{2} \right) \right] \times \left[\frac{1}{2} \pm \left(\frac{y}{\ell} - \frac{1}{2} \right) \right] \quad (39)$$

interpolates the field everywhere else over an element with edges of length ℓ . The sign \pm is taken positive for x when the value of i is 2 or 3, and positive for y when the value of i is 3 or 4. The small integrals over each element are carried in the local coordinate system

$$F_j(p) = \sum_{i=1}^4 G_{ij}(p) A_{ij} \quad (40)$$

where

$$G_{ij}(p) = 2 \text{ p.v.} \int_{\Sigma_j} E_k(q(x, y) - p) n(q(x, y)) f_i(x, y) dx dy. \quad (41)$$

For a single step in the iteration the Cauchy integral is calculated at every point p_m at the corners of every element. However, it is only necessary to evaluate the geometric components $G_{ij}(p_m)$ once, since the entire set of values does not change as the iteration proceeds. Gauss-Legendre integration [35] is used here to evaluate these values numerically. The calculations required for each iteration then amount to the product of a matrix $G'_j(p_m)$ and a vector A'_j

$$C_{\Sigma} u(p_m) = \sum_{j=1}^N \sum_{i=1}^4 G_{ij}(p_m) A_{ij} = \sum_{j=1}^{N+2} G'_j(p_m) A'_j \quad (42)$$

both of which contain Clifford-valued quantities. The vector A_{ij} contains multiple copies of the points at the corners of the elements. The values in the matrix $G'_j(p_m)$ are obtained from the matrix $G_{ij}(p_m)$ by adding together columns which operate on common points. For any particular problem the matrix is fixed, and the vector A'_j represents the most recent estimate of the field at all $N + 2$ points on the boundary.

A. Numerical Tests

The iterative algorithm has been investigated by performing numerical tests exposing a cube of 1 m^3 with edges aligned to the axes of a Cartesian system to two different incident fields.

In the first case the incident field is a uniform plane wave travelling in the positive z direction, written in terms of electric and magnetic fields as [33]

$$\begin{cases} \vec{E}(x, y, z) = E_x \vec{a}_x = E_0 e^{-j\beta z} \vec{a}_x \\ \vec{H}(x, y, z) = H_y \vec{a}_y = H_0 e^{-j\beta z} \vec{a}_y \end{cases} \quad (43)$$

Numerical values of $E_0 = 120\pi \text{ V/m}$ and $H_0 = 1 \text{ A/m}$ were taken for the magnitude of electric and magnetic fields respectively, and a numerical value of $\beta = 1 \text{ rad/m}$ for the wavenumber.

In the second case the incident field emanates from a Hertzian dipole source oriented in the positive z direction at the center of the cube, written in terms of electric and magnetic fields in spherical coordinates as [33]

$$\begin{cases} \vec{H}(x, y, z) = H_{\phi} \vec{a}_{\phi} = \frac{I_0 \ell}{4\pi} e^{-j\beta r} \left(\frac{j\beta}{r} + \frac{1}{r^2} \right) \sin \theta \vec{a}_{\phi} \\ \vec{E}(x, y, z) = E_r \vec{a}_r + E_{\theta} \vec{a}_{\theta} = \frac{I_0 \ell}{4\pi} e^{-j\beta r} \\ \times \left[\left(\frac{2\eta}{r^2} + \frac{2}{j\omega\epsilon r^3} \right) \cos \theta \vec{a}_r + \left(\frac{j\omega\mu}{r} + \frac{1}{j\omega\epsilon r^3} + \frac{\eta}{r^2} \right) \sin \theta \vec{a}_{\theta} \right] \end{cases} \quad (44)$$

A numerical value of $I_0 \ell = 0.04 \text{ Am}$ was taken for the strength of the dipole, and a numerical value for the wavenumber of $\beta = 1 \text{ rad/m}$.

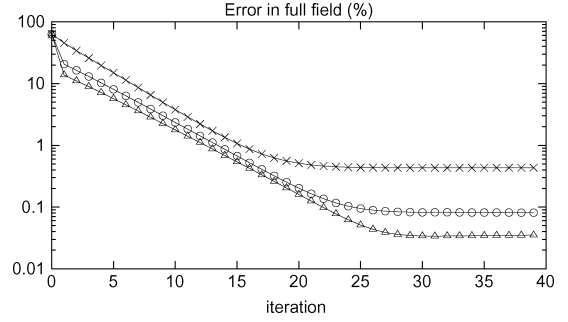


Fig. 9. Percentage error in full field during iteration towards plane wave solution. Boundary elements N : \times 150, \circ 384, \triangle 600.

In both cases free space values were taken for electric permittivity ϵ , magnetic permeability μ and intrinsic impedance $\eta = \sqrt{\mu/\epsilon}$. All of the calculations are carried using Clifford arithmetic, but the results are converted to vector form so they can be compared more easily to standard formulæ, such as in [33].

The tests aim to construct the full transmitted field $u = u^+$ on the boundary from half of the incident field ($f, \vec{n} \cdot \vec{E}$ and $\vec{n} \times \vec{H}$) using the iterative algorithm of Fig. 6. Once the full field on the boundary is constructed it can be extended using the Cauchy extension, for the first case into the region bounded by the cube and for the second case into the unbounded region outside the cube, as shown in [24].

Errors in the solution are presented in two forms. For the full field over the entire cube the error is presented as a single average value

$$\% \text{ error} = 100 \sum_{i=1}^{N+2} \sqrt{\frac{\mu(\Delta\zeta_i)^2 + \epsilon(\Delta\xi_i)^2}{\mu\zeta_i^2 + \epsilon\xi_i^2}} \quad (45)$$

where N is the number of elements, and

$$\begin{cases} (\Delta\zeta)^2 = \Delta\vec{H} \cdot \Delta\vec{H}^* = |\Delta H_x|^2 + |\Delta H_y|^2 + |\Delta H_z|^2 \\ (\Delta\xi)^2 = \Delta\vec{E} \cdot \Delta\vec{E}^* = |\Delta E_x|^2 + |\Delta E_y|^2 + |\Delta E_z|^2 \end{cases} \quad (46)$$

are the errors in the magnitudes of the complex field vectors at the $N + 2$ distinct corners of the elements, and

$$\begin{cases} \zeta^2 = \vec{H} \cdot \vec{H}^* = |H_x|^2 + |H_y|^2 + |H_z|^2 \\ \xi^2 = \vec{E} \cdot \vec{E}^* = |E_x|^2 + |E_y|^2 + |E_z|^2 \end{cases} \quad (47)$$

are the magnitudes of the complex field vectors of the known solution at the same points.

For the individual components of the field at individual points (in either Cartesian or spherical coordinates) the complex value of the error is presented in two parts, one part in phase with and one part in quadrature to the expected complex value, as a percentage of the magnitude of the whole \vec{E} or \vec{H} field.

VIII. NUMERICAL RESULTS

A. Case 1: Plane Wave

For the first case, Fig. 9 shows the error in the full field decreasing as the iterative algorithm progresses towards the solution. The three curves are for different conditions, with the cubic boundary divided into either $N = 150, 384$ or 600 elements. With each condition the solution obtained has a finite error. The error decreases as the number of boundary elements

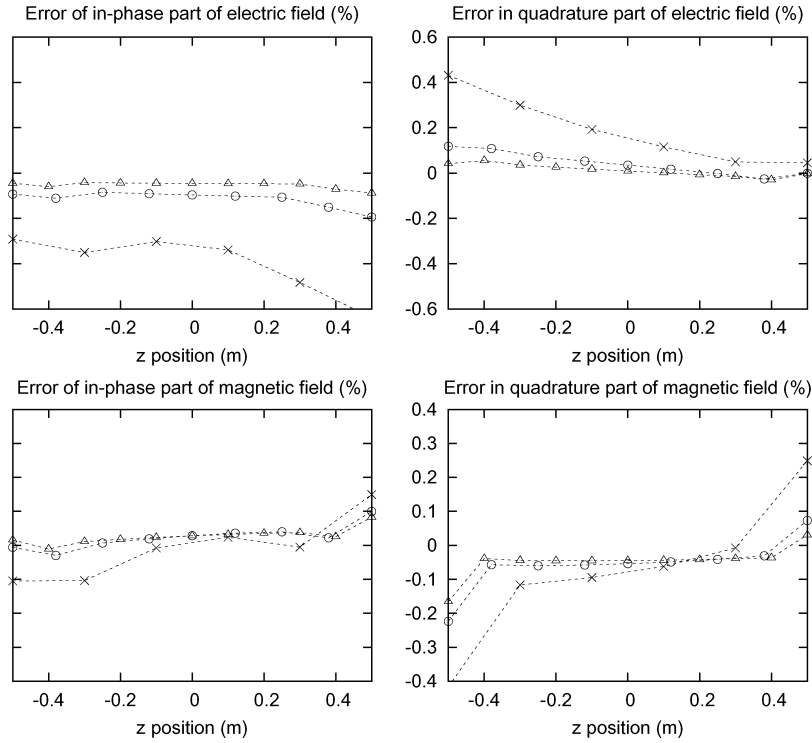


Fig. 10. Error in electric and magnetic field components on edge of cube for plane wave source. Upper: E_x , lower: H_y . Left: in-phase, right: quadrature. Boundary elements N : \times 150, \circ 384, \triangle 600.

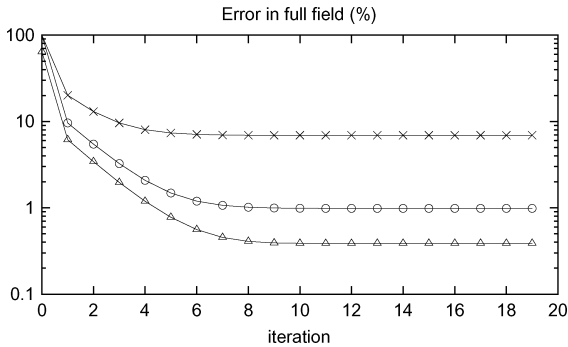


Fig. 11. Percentage error in full field during iteration towards dipole solution. Boundary elements N : \times 150, \circ 384, \triangle 600.

is increased. The error is slightly below 0.04% when the number of boundary elements $N = 600$.

Fig. 10 shows at the 39th iteration the errors in the electric and magnetic fields along one edge of the cube ($x = y = -(1/2)$). The errors along the edge are in broad agreement with the values in Fig. 9. However, the errors at the corners themselves tend to be higher than average. This is more noticeable for the magnetic field, where they are in the vicinity of 0.1% when 600 boundary elements are used.

B. Case 2: Hertzian Dipole

For the second case, Fig. 11 shows the error in the full field decreasing as the iterative algorithm progresses towards the solution. The three curves are for different conditions, with the cubic boundary divided into either $N = 150, 384$ or 600 elements. With each condition the solution obtained has a finite error. The error decreases as the number of boundary elements

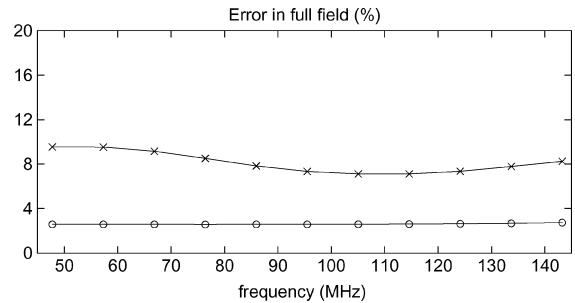


Fig. 12. Error in far field at $r = 628.3$ m, $\theta = 90^\circ$ and $\phi = 0^\circ$ generated by all components E, H of near field \circ , and generated by components E_n, H_t of near field \times .

is increased. The error is slightly below 0.4% when the number of boundary elements $N = 600$.

At the 19th iteration the errors in the electric and magnetic fields along the edge of the cube (not shown) are in broad agreement with the values in Fig. 11. In some cases, such as the radial electric field E_r and the magnetic field H_ϕ , the errors at the corners are higher. However, that is not exclusively the case. For the electric field E_θ the errors close to $z = 0$ are higher.

IX. APPLICATION

Fig. 12 shows the results of extending the near field of a dipole source measured on a cube of 1 m^3 to the far field at a point 623.8 m from the center of the cube using $N = 150$ boundary elements.

For the lower curve all components of the E and H fields are taken on the cube from the analytical formula for a dipole source (44) and the far field is constructed in a single step using the Cauchy extension (15). The error is due to the limited number of boundary elements (see [36]). For the upper curve, the normal

component E_n of the electric field and the tangential component H_t of the magnetic field are taken on the cube from the analytical formula. As a first step the missing components E_t and H_n are reconstructed using the iterative technique described in Section VI. As a second step the far field is constructed using the Cauchy extension. In this case the error includes that made during both steps of the calculation.

X. DISCUSSION

The iterative method presented in Section VI-B can be used for both perfectly reflective and transmissive interfaces. Here the tests are on the transmissive type of interface since the results are in general known in advance. This knowledge makes it easier to properly evaluate the performance of the algorithm.

The cube is chosen as a test shape for the reason of simplicity. For surfaces with sharp edges and corners it is usually expected that the field contains singularities at some points. That is not the case here, since the incident field is transmitted through the surface without perturbation. The field everywhere, including on edges and corners, is that of either a plane wave or is that of a dipole source. In the first case the field is totally void of singularities, and in the second case there is one singularity at the source itself. However, the dipole here is placed *off* the surface, so the field *on* the surface is everywhere finite and well behaved.

The accuracy achieved in Fig. 9 for the plane wave source is greater than in Fig. 11 for the dipole source. The orientation of the plane wave matches the orientation of the surface and also matches the orientation of the elements into which the surface is divided. The same is not true for the dipole source, where the nature of the wave is more well suited by a spherical rather than a cubic and Cartesian system. The bilinear functions and the quantization chosen here are set in the Cartesian framework, and do not accommodate the dipole field as easily as they accommodate the plane wave. It then follows for any given level of quantization that the accuracy is likely to be higher for the plane wave. Nevertheless, for both cases the accuracy can be improved by increasing the number of elements. It is likely that the same would also be the true if functions of higher order than bilinear were used.

The rate of convergence towards solution appears in Fig. 11 higher for the dipole source than in Fig. 9 for the plane wave, although the shape of the curve for the dipole makes it somewhat difficult to obtain a good estimate. For the plane wave, the accuracy accrues at a rate of one decimal place for every ten iterations. Five decimal places could be obtained with 50 iterations, although it would be necessary to use a higher number of elements than here.

In the case of Fredholm integral equations, the rate of convergence can be improved by replacing Neumann style iterative solutions by various alternatives, such as the conjugate gradient method (cf. [37]). It would be expected that similar improvements can be achieved if the same methods apply in the non-Fredholm non-commutative situation here.

For each iteration the computational effort is as for the multiplication of a matrix with $(N+2)^2$ elements onto a vector of $N+2$ elements, i.e. $(N+2)^2$ multiplications and additions. For $N = 600$ each iteration requires 362,404 operations. If indeed 50 iterations do give adequate accuracy, then the total computational effort is $50(N+2)^2$, which is less than a direct inverse of $(N+2)^3$ for all $N > 48$.

The operations of multiplication and addition are carried in Clifford arithmetic, which takes more work than real arithmetic. Without taking special short cuts, a Clifford multiplication of two four-dimensional Clifford numbers, each of which have 16 complex coefficients, takes $16^2 = 64$ complex multiplications and additions when implemented as 4×4 Dirac matrices. However, for applications in electromagnetism short cuts can be achieved because many of the 16 complex coefficients are zero. The \vec{E} and \vec{H} fields together require only six non-zero complex coefficients, and simple vectors such as the normal vector \vec{n} require only three non-zero real coefficients.

The mathematical theory [17], [18], [25], [34] behind the method presented here is quite rigorous. The implementation departs from the rigor of the theory by making three different approximations. Firstly, the surface is quantized into a finite number of elements (here squares). Secondly, the field on each element is supposed to conform to a particular generic form (here bilinear). Thirdly, integrals over the elements are evaluated numerically (here by Gauss Legendre integration). Such departures from the theory, if taken too far, can render its support invalid. However, if departures from the theory are kept within acceptable limits, valid solutions are guaranteed. Although it is not clear in general what those limits might be, the experience here is that valid solutions are achievable (within a fixed amount of error) using relatively simple approximations. Needless to say, making improvements to those approximations is likely to yield even more accurate results.

When converting an implementation of the transmissive problem into an implementation of the reflective problem as described in Section VI-B some care must be taken. Validity of the conversion relies on the resulting implementation meeting certain conditions required of the reflective solution, but not of the transmissive solution. In principle, basis functions which support singularities at the corners and edges are required. Use of bilinear functions as here cannot be expected to give optimal results. With the new basis functions, methods of integration must be chosen accordingly i.e. to support (integrable) singularities at the limits of the integration. Doing so eliminates the need for the angular ratios in Table II at the corners and edges of the cube which, in the case of the transmissive problem, are unknown.

Our ongoing work involves testing the solution to the reflective problem in the case of various basis functions. Preliminary results in the reflective case are much the same as shown here for the transmissive case.

ACKNOWLEDGMENT

The authors wish to thank Asst. Prof. Dr. T. Angkaew of the Department of Electrical Engineering at Chulalongkorn University for interesting discussions pertaining to the physical interpretation of some of the problems discussed in this paper. They would also like to thank Asst. Prof. Dr. Wanchai Pijitrojana of Thammasat University for his encouragement and support for this work.

REFERENCES

- [1] A. J. Poggio and E. K. Miller, "Integral equation solutions of three-dimensional scattering problems," in *Computer Techniques for Electromagnetics*, R. Mittra, Ed. New York: Pergamon, 1973, ch. 4, pp. 201–210.

[2] D. L. Colton and R. Kress, *Integral Equation Methods in Scattering Theory*. New York: Wiley Interscience, 1983.

[3] F. Alouges, S. Borel, and D. Levaudoux, "A stable well-conditioned integral equation for electromagnetism scattering," *J. Computat. Appl. Math.*, vol. 204, pp. 440–451, 2007.

[4] J. R. Mautz and R. F. Harrington, "H-field, E-field and combined-field solution for conducting bodies of revolution," *Arch. Elektron. Übertragungstech. (AEU)*, vol. 32, no. 4, pp. 157–164, Apr. 1978.

[5] D. J. Taylor, "Accurate and efficient numerical integration of weakly singular integrals in Galerkin EFIE solutions," *IEEE Trans. Antennas Propag.*, vol. 51, no. 7, pp. 1630–1637, Jul. 2003.

[6] A. F. Peterson and M. M. Bibby, "Error trends in higher-order discretizations of the EFIE and MFIE," in *Proc. Antennas and Propag. Society Int. Symp.*, Jul. 2005, vol. 3A, pp. 52–55.

[7] Ö. Ergül and L. Gürel, "Investigation of the inaccuracy of the MFIE discretized with RWG basis functions," in *Proc. Antennas and Propag. Society Int. Symp.*, Jun. 2004, vol. 3, pp. 3393–3396.

[8] Ö. Ergül and L. Gürel, "Improved testing of the magnetic-field integral equation," *IEEE Microw. Wireless Compon. Lett.*, vol. 15, no. 10, pp. 615–617, Oct. 2005.

[9] M. H. Smith and A. F. Peterson, "Numerical solution of the CFIE using vector bases and dual interlocking meshes," *IEEE Trans. Antennas Propag.*, vol. 53, no. 10, pp. 3334–3339, Oct. 2005.

[10] P. Ylä-Oijala and M. Taskinen, "Calculation of CFIE impedance matrix elements with RWG and $n \times$ RWG functions," *IEEE Trans. Antennas Propag.*, vol. 51, no. 8, pp. 1837–1846, Aug. 2003.

[11] R. J. Adams, "Combined field integral equation formulations for electromagnetic scattering from convex geometries," *IEEE Trans. Antennas Propag.*, vol. 52, pp. 1294–1303, 2004.

[12] X. Antoine and M. Darbas, "Generalised combined field integral equations for the iterative solution of the three-dimensional Helmholtz equation," *Math. Model. Numer. Anal.*, vol. 41, pp. 147–167, 2007.

[13] R. F. Harrington, *Field Computation by Moment Methods*. New York: Wiley-IEEE Press, May 1993.

[14] Q. Ye and L. Shafai, "Investigation of the projection iterative method in solving the MoM matrix equations in electromagnetic scattering," *IEE Proc. Microw. Antennas Propag.*, vol. 147, no. 6, pp. 445–450, 2000.

[15] T. F. Eibert, "Iterative near-zone preconditioning of iterative method of moments electric field integral equation solutions," *IEEE Antennas Wireless Propag. Lett.*, vol. 2, pp. 101–102, 2003.

[16] Q. Ye and L. Shafai, "Performances of projection iterative method on electromagnetic scattering by spheres," in *Proc. Antennas Propag. Society Int. Symp.*, Jun. 1998, vol. 3, pp. 1526–1529.

[17] A. McIntosh, "Clifford algebras and the higher-dimensional Cauchy integral," in *Approximation Theory and Function Spaces*, ser. BCP series, Z. Ciesielski, Ed. Warsaw, Poland: Banach Center Publications, 1989, pp. 253–267, no. 22.

[18] A. Axelsson, R. Grogard, J. Hogan, and A. McIntosh, "Harmonic analysis of Dirac operators on Lipschitz domains," in *Clifford Analysis and Its Applications*, ser. NATO Science Series II, Mathematics Physics and Chemistry, F. Brackx, Ed. Dordrecht: Kluwer, 2001, pp. 231–246.

[19] A. J. Burton and G. F. Miller, "The application of integral equation methods to the numerical solution of some exterior boundary-value problems," *Proc. Royal Society London*, vol. 323, pp. 201–210, 1971.

[20] G. C. Moisil and N. Théodorescu, "Fonctions holomorphes dans l'espace," *Mathematica Cluj*, vol. 5, pp. 142–159, 1931.

[21] W. K. Clifford, "Applications of Grassmann's extensive algebra," *Amer. J. Math.*, vol. 1, no. 4, pp. 350–358, 1878.

[22] M. Chisholm, *Such Silver Currents: The Story of William and Lucy Clifford 1845–1929*. Cambridge, U.K.: Lutterworth Press, Mar. 2002, p. 28.

[23] A. C. Laseby, C. Doran, and E. Arcaute, "Applications of geometric algebra in electromagnetism, quantum theory and gravity," in *Proc. 6th Int. Conf. on Clifford Algebras and Their Applicat.*, R. Ablamowicz, Ed., 2003, no. 476.

[24] C. Ajalawit, A. Seagar, and T. Angkaew, "Calculation of electromagnetic field with integral equations based on Clifford algebra," in *Proc. Progr. in Electromagn. Res. Symp. (PIERS'07)*, Aug. 2007, pp. 62–71.

[25] A. Axelsson, "Transmission Problems for Dirac's and Maxwell's Equations With Lipschitz Interfaces," Ph.D. dissertation, Australian National Univ., Canberra, Australia, Nov. 2002.

[26] A.-S. B.-B. Dhia, C. Hazard, and S. Lohrengel, "A singular field method for the solution of Maxwell's equations in polyhedral domains," *SIAM J. Appl. Math.*, vol. 59, pp. 2028–2044, 1999.

[27] C. Hazard and S. Lohrengel, "A singular field method for Maxwell's equations: Numerical aspects for 2D magnetostatics," *SIAM J. Numer. Anal.*, vol. 40, no. 3, pp. 1021–1040, 2002.

[28] D. Mitrea and M. Mitrea, "Finite energy solutions of maxwell's equations and constructive hodge decompositions on nonsmooth riemannian manifolds," *J. Functional Anal.*, vol. 190, no. 2, pp. 339–417, 2002.

[29] V. L. Hansen, *Functional Analysis—Entering Hilbert Space*. Englewood Cliffs, NJ: World Scientific, 2006.

[30] P. Lounesto, *Clifford Algebras and Spinors*, ser. London Mathematical Society Lecture Notes, 2nd ed. Cambridge, U.K.: Cambridge Univ. Press, 2008.

[31] A. McIntosh and M. Mitrea, "Clifford algebras and Maxwell's equations in Lipschitz domains," *Mat. Methods Appl. Sci.*, vol. 22, no. 18, pp. 1599–1620, 1999.

[32] D. Hestenes, "Oersted medal lecture 2002: Reforming the mathematical language of physics," *Amer. J. Phys.*, vol. 71, pp. 101–121, 2003.

[33] C. A. Balanis, *Advanced Engineering Electromagnetics*. New York: Wiley, May 1989.

[34] A. McIntosh, "Clifford algebras, Fourier theory, singular integrals and harmonic functions on Lipschitz domains," in *Clifford Algebras in Analysis and Related Topics*, ser. Studies in Advanced Mathematics, J. Ryan, Ed. Boca Raton, FL: CRC press, 1996, vol. 21, pp. 33–87.

[35] W. H. Press, S. A. Teukolsky, W. T. Vetterling, and B. P. Flannery, *Numerical Recipes—The Art of Scientific Computing*, 3rd ed. Cambridge, U.K.: Cambridge Unvi. Press, Sep. 2007.

[36] C. Ajalawit and T. Angkaew, "Numerical computation of electromagnetic far-field from near-field using integral equation based on Clifford algebra," in *Proc. Asia Pacific Microw. Conf. (APMC'07)*, Dec. 2007, pp. 1–4.

[37] M. Yuan, P. M. van den Berg, and T. K. Sarkar, "Direct extrapolation of a causal signal using low-frequency and early-time data," *IEEE Antennas Propag. Mag.*, vol. 53, no. 7, pp. 2290–2298, Jul. 2005.



Ajalawit Chantaveerod received the Bachelor and Masters degrees in electrical engineering from the Prince of Songkla University, Thailand, in 2002 and 2004, respectively. He is currently working toward the Ph.D. degree in electrical engineering at Chulalongkorn University, Bangkok, Thailand. He is also working as a Lecturer at Walailak University, Southern Thailand.



Andrew D. Seagar (M'82) received the Bachelor and Ph.D. degrees in electrical engineering from the University of Canterbury, New Zealand, in 1978 and 1983, respectively. He has worked in various full time research, industry and university positions in England, Australia, Canada and Thailand.